Improvement of the electrochemical behavior of (Sb, Sn, Cu)O ceramic electrodes as electrochemical advanced oxidation anodes

J.J. Giner-Sanz[a], M.J. Sánchez-Rivera[b], M. García-Gabaldón[a], E.M. Ortega[a], S. Mestre[b], V. Perez-Herranz*[a]
[a] Dr. J.J. Giner-Sanz;, Dr. M. García-Gabaldón, Dr. E.M. Ortega, Prof. V. Perez-Herranz
IEC group, Depto. Ingeniería Química y Nuclear
Universitat Politècnica de València,
Valencia, Spain.
E-mail: vperez@iqn.upv.es
[b] M.J. Sánchez-Rivera, Dr. S. Mestre
University Institute of Ceramic Technology
Universitat Jaume I
Castellón, Spain

Abstract: This work explores the possibility of increasing the active surface of a Sb-doped SnO_2 ceramic electrode using CuO as sintering aid, by incorporating petroleum coke as a pore generator. In order to fulfil this goal, three series of (Sb,Sn,Cu)O electrodes with different coke contents, were synthetized. The properties of the electrodes, and their microstructure, change significantly as a function of the coke content before sintering. The electrochemical characterization of the synthetized electrodes showed that the coke addition before sintering causes two antagonist effects on the performance of the (Sn,Sb,Cu)O electrodes as electrochemical advanced oxidation processes (EAOP) anodes. On the one hand, it significantly improves the electrochemical roughness factor of the electrode, solving in this way the densification problem. On the other hand, it worsens the electrochemical behavior of the electrode: narrowing its electrochemical window; and "activating" it slightly: the addition of coke before sintering changes the kinetic parameters, leading to a kinetic situation in which the accumulation of hydroxyl radicals is slightly lower. A balance must be sought: an intermediate coke content will improve significantly the electrochemical roughness factor of the electrode, but will only worsen slightly its electrochemical behavior, leading to an optimum (Sn,Sb,Cu)O EAOP anode.

Keywords: Antimony-doped tin oxide electrodes; Ceramic anodes; Electrooxidation process; Petroleum coke; Pore generator

ARTICLE

Sb-doped SnO_2 ceramic electrodes were synthesized, using CuO as sintering aid, and incorporating different amounts of petroleum coke as a pore generator. It was shown that an intermediate coke content improves significantly the electrochemical roughness factor of the electrode, but only worsens slightly its electrochemical activity for generating hydroxyl radicals, leading to an optimum (Sn,Sb,Cu)O electrochemical advanced oxidation anode.

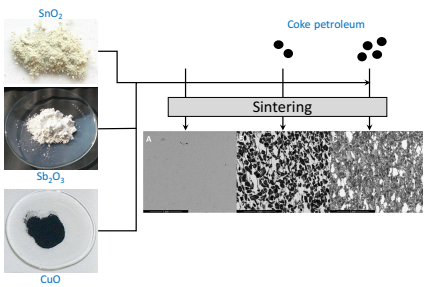

*J.J. Giner-Sanz, M.J. Sánchez-Rivera, M. García-Gabaldón, E.M. Ortega, S. Mestre, V. Perez-Herranz**

Page No. – Page No.

Improvement of the electrochemical behavior of (Sb, Sn, Cu)O ceramic electrodes as electrochemical advanced oxidation anodes

Introduction

In the last decades, there has been an astronomical increase of the drinking water demand, due to the exponential growth of the World's human population [1]. For this reason, the protection of the integrity of the water resources has become one of this century's critical environmental issues. One of the main current worldwide concerns is the growth of water pollution by organic compounds arising from human activities [2]. The vast majority of them are persistent organic pollutants (i.e. recalcitrant pollutants), owing to their resistance to conventional wastewater treatments [3]. As a result, these compounds are building up in nearly every water body of the planet: they have been detected in rivers, lakes, oceans and even drinking waters all over the world. Due to their toxicity and potential hazardous health effects (v.g. carcinogenicity and mutagenicity) on living organisms, including human beings, their accumulation constitutes a serious environmental health problem.

Since the late 80's, a large number of research teams have focused on developing more effective technologies to totally remove recalcitrant organic pollutants from wastewaters. A wide range of alternative processes have been studied in this context. Among them, advanced oxidation processes (AOPs) have emerged as interesting alternatives [4]. The efficiency of these processes for removing recalcitrant pollutants from wastewaters has been widely reported in literature for a vast variety of recalcitrant pollutants [5]: pharmaceuticals, such as Propranolol and Diatrizoate [6-8]; dies, like Disperse Blue 3 [9, 10]; pesticides and herbicides, such as Tebuthiuron and glyphosate [11, 12]; and industrial compounds, like Phenol, Bisphenol A and EDTA [13-16].

Electrochemical advanced oxidation processes (EAOPs) are a particular type of AOPs that have gained increasing attention [17]. This technology uses electrical energy as a vector for environmental decontamination: the organic compounds are degraded either by direct electron transfer to the anodic electrode (i.e. direct oxidation pathway), or by oxidants that have been electrochemically generated in situ (i.e. indirect oxidation pathway) [18]. The wide diversity of effluents that have been successfully treated with this technology shows its great efficiency and flexibility [19]. One of the key components of an EAOP is its anodic electrode, which should be a stable and cheap "inactive" anode [20]. In the EAOP context, "active" anodes contain transition elements (v.g. Pt) on their surfaces, which enhance the oxygen evolution reaction (OER) and the direct partial oxidation of pollutants. In this kind of anodes, the OER intermediates (v.g. hydroxyl radicals) are adsorbed on the anode's surface, confining the oxidation to the surface of the electrode [21]. This makes "active" anodes mostly unsuitable for mineralizing complex organic substances [20]. On the contrary, "inactive" anodes lead to the accumulation of hydroxyl radicals in the OER pathway. These strong oxidizing mediators favor the complete mineralization of organic compounds throughout an indirect mechanism [21]. Concerning "inactive" anodes, boron doped diamond (BDD) anodes are the actual state-of-the-art, since they possess a unique role towards the formation of ·OH radicals [22]. Despite their great electrochemical behavior in the EAOP context, these anodes have not reached a full implementation at industrial scale due to their high cost and low manageability [21].

Ceramic electrodes based on SnO_2 have been reported in literature as promising alternatives to the actual state-of-the-art EAOP anodes (i.e. BDDs) [23]. SnO_2 has a high ability for generating hydroxyl radicals, compared with Pt and other dimensionally stable anodes. However, pure SnO_2 electrodes have limited application, due to the low conductivity of this semiconductor material. This limitation has been overcome by using antimony as a dopant [24]. Nowadays, Sb-doped SnO_2 electrodes are thought to be superior EAOP anodes [25]. However, ceramic SnO_2-based electrodes present a major drawback: their poor sinterability [26]. This limitation has prevented their full implementation at industrial scale. In literature two methods have been proposed in order to tackle this problem: the use of special sintering techniques [27], such as the Field Activated Sintering Technique (FAST) [28]; or the use of sintering aids, such as copper, zinc and manganese oxides [29]. CuO is a common choice for Sb-doped SnO2 anodes, since it has a moderate cost and presents excellent sintering aid properties [30]. Unfortunately, the use of CuO as sintering aid leads to heavily densified anodes. And it is a well-known fact in the electrochemistry field, that a key aspect in order to increase the degradation efficiency of a given EAOP anode, is to increase its specific

area and the number of active sites [31]. Therefore, the use of copper oxide as sintering aid solves the sintering problem, at the cost of significantly worsening the electrochemical properties of the EAOP anode.

This work aims to explore the possibility of mitigating this drawback by increasing the active surface of a Sb-doped SnO_2 electrode sintered using CuO as sintering aid, by incorporating petroleum coke as a pore generator. There are many pore generators described in the literature, mainly organic compounds as starches [32]. However, their mechanical behavior along the dry-pressing process is very different from the SnO_2-based mixture one, generating defects in the specimens like cracks. In addition, starches also introduce impurities in the system, whose proportion and characteristics are function of their origin [33]. Conversely, high quality petroleum coke has a very low level of impurities and its mechanical behavior during pressing allows shaping the green electrodes by dry-pressing without defects. In order to analyze the viability of petroleum coke as pore generator, a series of (Sb,Sn,Cu)O electrodes with 3 different coke contents, was synthetized. First, the electrodes were characterized from a physical and a morphological point of view. Then, a complete electrochemical characterization was performed in order to obtain several parameters that are relevant for the characterization of the performance of the electrodes as EAOP anodes: the electrochemical window, the electrochemical rugosity factor, and the oxygen evolution reaction (OER) Tafel parameters. The results were compared with analogue results obtained for an "active" anode (i.e. Pt), and for a current state-of-the-art "inactive" anode (i.e. BDD).

Results and Discussion

Physical and morphological analysis

The addition of coke before sintering has a significant impact on the electrode's densification and on its porosity (figures 1 and 2). Coke-free specimens show high densification and lack of open porosity. As the coke content increases, a decrease in the densification of the specimens is observed, experiencing up to an 86% reduction in densification between coke-free specimens and those containing the maximum percentage of coke (i.e. 40 wt.%). The total pore volume shows an opposite trend: it increases as the coke content is higher. Obviously, coke is a material whose particles burn before the sintering process, leaving a porous network in its place. However, their effects over densification and total volume of pores were not completely linear, as some deviations were detected for contents of pore generator higher than 20 wt.%. On the other hand, the pore size distribution of the sintered electrodes supports that the effects of coke are different depending of its content (figure 3). A practically monomodal distribution is observed in the case of the composition with 20 wt.% of coke, with a mean pore size around 10 µm. However, when coke proportion is increased up to 40 wt.%, the pore size distribution is wider and trimodal, with pores distributed in three intervals of sizes, centered around 5, 10 and 100 µm respectively. Considering that the mercury intrusion technique measures the minimum diameter of the access channel as the size of each pore, that results can be interpreted. Moderate proportions of coke generate pores whose connections with the outside are channels of approximately the same diameter. However, high proportions of coke generate channels of different diameters as there is a higher probability that coke particles remain in the shaped specimen in close contact as agglomerates.

The microstructure of the different electrodes is consistent with the previous interpretation (figure 4). The coke-free specimens present a highly densified structure with a low proportion of isolated small rounded pores (figure 4.A), which is consistent with the obtained value of densification (almost 95%). In the case of electrodes with a 20 wt.% of coke, the image shows a totally different microstructure, with a high porosity composed of pores of irregular shape (related to the initial shape of the coke particles), with a size around 100 µm distributed in groups. Between the groups, some islands of well-sintered ceramic are present, but they show numerous cracks (figure 4.B). Finally, when the percentage of coke is 40 wt.%, the microstructure becomes very heterogeneous because it looks like a sponge (figure 4.C), the pores have lost the individuality appreciated in figure 4.B and the islands of

densified ceramic are fewer and smaller. Obviously, the microstructure changes with the proportion of coke are reflected in the densification of the electrode and in its pore size distribution.

The energy-dispersive X-ray (EDX) analysis of the samples (figure 5), showed clearly the effect of the coke addition. The peak corresponding to the carbon increases with coke's percentage, because a greater proportion of the resin (used to fix the sample during the polishing process) infiltrates through the porous network. In the case of the sample manufactured with 40 wt.% of coke, a small peak corresponding to chlorine, also present in the resin used, was detected. However, it was not possible to quantify the elements present in each electrode with enough precision. In fact, the proportions of Cu and Sb in the samples were below (Cu) or around (Sb) the detection limit of the EDX equipment in the operation conditions used in this study. In addition, there is a strong overlapping between secondary peaks of Sn and the peaks of Sb, including its main peak, which increases the uncertainty of the measurement.

In opposition to the improvement of porosity, coke has an unfavorable effect on the electrical resistivity (figure 6). The created pores restrict the movement of charge carriers. The significant changes in the microstructure lead to differences of some orders of magnitude in the aforementioned electrical property. The addition of coke in proportions higher than 20 wt.% causes an excessive increase in the electrical resistivity, as the paths for electrical conductivity are restricted by the spongy microstructure. In consequence, high proportions of coke generate unsuitable electrodes for this specific application.

Electrochemical characterization

Figure 7 presents the CVs obtained for each electrode at a scan rate of 40 $mV \cdot s^{-1}$. On the one hand, subfigure a represents the current density referred to the geometric area; and on the other hand, subfigure b represents the current density referred to the active surface. As it can be observed in figure 7.a, for a given applied potential, the geometric current density of the ceramic electrodes falls between the geometric current density of the Pt anode, which displays the maximum current density; and the geometric current density of the BDD anode, which displays the minimum current density. Comparing the ceramic electrodes with each other, it can be observed that at a given applied potential, the geometric current density increases with the coke content before the sintering. In order to determine whether this trend can be fully explained by differences in the rugosity factor (i.e. active area per geometric area), the current densities referred to the active surface have to be compared. The same trends that were observed in figure 7.a, can be identified in figure 7.b. Therefore, the current densities referred to the active surface display the same trends than the current densities referred to the geometric surface. This observation implies that the differences observed in the geometric current densities cannot be fully explained by the difference in the electrochemical rugosity factor of the different electrodes; and that therefore, the 5 anodes present different OER intrinsic apparent activities. It should be noted that even though the active surface current densities of the ceramic electrodes present differences; these differences are significantly smaller than the differences observed in the geometric current densities. This implies that a big fraction of the differences in the geometric current densities are explained by the rugosity factor; and only a little fraction is due to differences in the apparent intrinsic activity of the electrodes. For the sake of clarity, in this work only the CVs obtained for one of the scan rates (40 $mV \cdot s^{-1}$) are presented. However, the trends observed for 40 $mV \cdot s^{-1}$ were also observed in the other 9 scan rates, and in the steady state curves.

Several conclusions on the activity of the different electrodes can be extracted from the aforementioned observations. First, the well-known fact that the Pt electrode is the most "active" anode among the 5 considered electrodes, and the BDD electrode is the most "inactive" one. Second, the ceramic electrodes present intermediate activities that are significantly closer to the BDD's activity than to the Pt one. This is the reason why the (Sn, Sb, Cu)O electrodes are potential EAOP anodes. Third, the addition of coke before sintering leads to a slightly more "active" anode. In other words, the addition of coke before sintering increases the apparent intrinsic activity of the ceramic electrode, making its electrochemical behavior less similar to the BDD's one. It is well-

known that a lower anode activity leads to a larger accumulation of strong oxidizing OER intermediates (v.g. hydroxyl radicals); and therefore, favors the organic compound mineralization [21]. Hence, the addition of coke before sintering slightly worsens the electrochemical behavior of the (Sn, Sb, Cu)O electrode as an EAOP anode, in the electrode activity context.

Figure 8 shows the OCP of the different electrodes. The first observation that can be extracted from the aforementioned figure, is that the ceramic electrodes present significantly higher OCPs than the Pt electrode and the BDD electrode. Moreover, the OCP presents a negative trend with the coke content before sintering: the (Sn, Sb, Cu)O electrode with no coke displays a higher OCP than the 20% coke electrode, which in turn displays a higher OCP than the 40% coke electrode. This observation shows that the pore generator modifies the open-circuit electrochemical behavior of the anode.

The electrochemical rugosity factor is another relevant parameter for assessing the performance of a given electrode as an EAOP anode. This parameter is defined as the ratio between the real active surface of an electrode and its geometric area. In this work, the following expression was used in order to calculate the factor of the considered ceramic electrodes:

$$\gamma = \frac{Q_{total}}{Q_{out}} = \frac{Q_{out} + Q_{in}}{Q_{out}} \qquad (1)$$

Where denotes the “outer” charge, related to the more accessible surface; and is the “inner” charge, related to the less accessible surface. The “total” charge is given by the sum of the “inner” and “outer” charges. In this work, and were obtained for each electrode from the voltammetric charge analysis of the CVs measured at 10 different scan rates, using the methodology proposed by Ardizzone and his co-workers [34].

Figure 9 gives the electrochemical rugosity factor obtained for the 3 considered (Sn, Sb, Cu)O electrodes. It can be clearly observed that the electrochemical rugosity factor increases when the coke content before sintering is increased: the 20% coke electrode presents a factor 30% higher than the electrode with no coke; and the 40% coke electrode presents a factor nearly 250% higher than the electrode with no coke. Therefore, coke presents very good pore generator properties: the generated pores increase the active surface of the electrode. Moreover, the electrochemical rugosity factor presents a clearly nonlinear relation with the coke content. These electrochemical rugosity factor values are consistent with the microstructures of the electrodes (figure 4). When the pores are grouped and communication channels between them are wider, the electrochemical rugosity factor increases. Since the common practice in electrochemistry is to try to maximize the active surface for a given geometric area, the coke addition before sintering improves the performance of the ceramic electrode with respect to its active surface.

Another relevant parameter for characterizing EAOP anodes is the oxygen evolution potential (OEP), which can be obtained from the steady-state polarization curves. Its importance relies on the fact that this parameter defines the electrochemical window of the electrode. By definition, the OEP is the electrode potential from which the generation of oxygen becomes significant. Since this definition is a rather fuzzy one, the common practice is to define it as the intersection of the tangent to the steady-state polarization curve at high anodic potentials, and the applied potential axis [23]. Using this definition, the OEP values of the different electrodes were obtained. Figure 10 shows the obtained results. The OEP values determined in this work for the Pt electrode, for the BDD electrode and for the ceramic electrodes, are consistent with the values available in literature for similar electrodes [21, 23, 35]. It can be observed that the Pt electrode has the lowest OEP among the 5 electrodes, while the BDD electrode has the highest one. The ceramic electrodes present intermediate OEPs. Comparing the ceramic electrodes between them, it can be observed that the 20% coke electrode presents an OEP 4% lower than the electrode with no coke; and the 40% coke electrode presents an OEP nearly 40% lower than the

electrode with no coke. Therefore, the OEP decrease presents a nonlinear relation with the coke content. Moreover, all three ceramic electrodes present OEP values significantly lower than the OEP of the BDD electrode. It is well-known that in the EAOP context, wide electrochemical windows (i.e. high OEP) are sought [36, 37]. Consequently, the addition of coke before sintering worsens the performance of the ceramic electrode as an EAOP anode, in terms of its electrochemical window: only a slight worsening occurs when the coke content is 20%, whereas the worsening is much more severe when the coke content is 40%.

Finally, figure 11 presents the I-R corrected pseudo-steady-state polarization curves of the 3 ceramic electrodes in the Tafel plane: overpotential versus The first observation that can be extracted from the aforementioned figure, is that all 3 ceramic electrodes present clear Tafel domains for overpotencials over 50 mV. Table 1 presents the OER Tafel parameters of each ceramic electrode. It can be observed that the 0% electrode and the 20% electrode display the same Tafel slope (b), 240 $mV \cdot dec^{-1}$; while the 40% electrode displays a lower Tafel slope, 133 $mV \cdot dec^{-1}$. These Tafel slopes are anomalously high. It is well-known that porous electrodes can present Tafel slopes as high as twice the Tafel slope of an analogue non-porous electrode [38]. Therefore, the anomalously high Tafel slopes observed in this work are due to the fact that the ceramic electrodes considered here are porous electrodes. In the 40% case, the pore properties (i.e. big pores) reduce the effect of the pores on the Tafel slope: the pores increase the active area, but their characteristics make the Tafel slope behave more like a non-porous electrode. For this reason, in the 40% electrode, the apparent Tafel slope is nearer to the real Tafel slope, which is the same in the 3 ceramic electrodes, and is equal to around 120 $mV \cdot dec^{-1}$. Therefore, the OER mechanism is the same in the 3 cases. The following OER mechanism on the (Sn, Sb, Cu)O electrodes can be proposed, based on the fact that the Tafel slope is equal or higher to 120 $mV \cdot dec^{-1}$ [21]:

$$S + H_2O_{(l)} \leftrightarrow S(H_2O)_{ads} \quad \textit{(R1)}$$

$$S(H_2O)_{ads} \leftrightarrow S(\cdot OH)_{ads} + H^+_{(ac)} + e^- \quad \textit{(R2)}$$

$$S(\cdot OH)_{ads} \leftrightarrow S(\cdot O)_{ads} + H^+_{(ac)} + e^- \quad \textit{(R3)}$$

$$S(\cdot O)_{ads} + H_2O_{(l)} \leftrightarrow S(\cdot OOH)_{ads} + H^+_{(ac)} + e^- \quad \textit{(R4)}$$

$$S(\cdot OOH)_{ads} \leftrightarrow S(O_2)_{ads} + H^+_{(ac)} + e^- \quad \textit{(R5)}$$

$$S(O_2)_{ads} \leftrightarrow S + O_2 \quad \textit{(R6)}$$

Where denotes an active site on the surface of the electrode, represents a chemical radical, and subscript ads refers to adsorbed intermediate species on the surface. Reaction (R3) is the rate-limiting reaction in this case, since the Tafel slope is equal or higher to $mV \cdot dec^{-1}$ [39]. This favors the accumulation of hydroxyl radicals which is what is wanted in an EAOP anode. Therefore, the 3 considered ceramic electrodes are feasible candidates for being EAOP anodes.

Although the mechanism is the same in the 3 ceramic electrodes, the kinetic parameters are not, as it can be deduced from the different values of the exchange current density As it can be seen in table 1, the exchange current density, though being of the same order of magnitude in the 3 cases, presents a positive relation with the coke content: when the coke content is increased, the exchange current density increases. This confirms the

observations extracted from the CVs and the pseudo-steady-state polarization curve: the addition of coke slightly "activates" the electrode, worsening its performance as EAOP anode in the "activity" context. Consequently, the addition of coke does not change the OER mechanism, but it does change the kinetic parameters, leading to a kinetic situation in which the accumulation of hydroxyl radicals is slightly lower.

Conclusions

In conclusion, petroleum coke is a good pore generator for (Cu,Sb,Sn)O electrodes, in order to compensate their high sinterability. On the one hand, the physical and morphological analysis showed that an increase in the coke content before sintering produces two effects on the physical properties: it increases both, the electrode porosity and its electrical resistivity. The first is a desirable effect, whereas the latter is an undesirable effect. These results suggest that an intermediate coke content should be used in order to increase the electrode porosity without causing an unacceptable increase in the electrical resistivity.

On the other hand, the electrochemical characterization showed that the addition of coke before sintering has two antagonist effects on the performance of the (Sn, Sb, Cu)O electrode as an EAOP anode. It significantly improves the electrochemical roughness factor of the electrode, at the expense of worsening its electrochemical properties. On the one side, an increase in the coke content before sintering narrows the electrochemical window of the electrode. On the other side, it "activates" the electrode: though it does not change the OER mechanism, it does change the kinetic parameters, leading to a kinetic situation in which the accumulation of hydroxyl radicals is slightly lower. Both, the positive and the negative effects, present a nonlinear relation with the coke content. Consequently, a balance has to be sought: an intermediate coke content will improve significantly the electrochemical roughness factor of the electrode, but will only worsen slightly its electrochemical behavior, leading to an optimum (Sn, Sb, Cu)O EAOP anode.

Experimental Section

Electrode synthesis and physical analysis

The electrodes were synthesized with SnO_2 as the main component (purity 99.85%, Quimialmel® S.A., Spain), Sb_2O_3 as a dopant (purity 99%, Alfa-Aesar®, Germany), and CuO as a sintering aid (purity 97%, Panreac® S.A., Spain), in molar percentages of 97.8 mol.%, 1.0 mol.% and 1.2 mol.% respectively. Three mass percentages of petroleum coke (0 wt.%, 20 wt.% and 40 wt.%) were tested to evaluate its behaviour as pore generator. Every one of the studied compositions included an additional 0.8 wt.% of polyvinylalcohol (Mowiol® 8-88, Clariant® Iberica S.A. Spain), as a ligand.

The electrodes were manufactured through the traditional ceramic method (no special technique was employed for shaping or sintering the specimens). The raw materials were mixed using water as a fluid in a planetary mill working at 230 rpm for one hour (Pulverisette® 5, Fritsch® GmbH, Germany). The obtained suspension was dried in an oven at 110℃ for 24 h. The dry powder was sieved trough a 600 µm mesh and moistened to 5.0% (kg water/kg dry solid). Prismatic specimens of 40x5x5 mm were shaped by dry pressing in a laboratory uniaxial manual press (Robima® S.A., Spain), working at 250 $kg \cdot cm^{-2}$. Finally, the samples were sintered in a laboratory furnace (RHF1600, Carbolite® Furnaces Ltd., UK). Coke-free specimens were sintered with a simple cycle (heating at 5℃ $\cdot\, min^{-1}$) until 1200℃ with a soaking time of 1 h and natural cooling to room temperature). However, coke-containing specimens required a specific thermal cycle which allows the complete oxidation of the pore generator before sintering (heating from room temperature to 200℃ at 10℃ $\cdot\, min^{-1}$, 1 hour of soaking time, heating from 200℃ to 300℃ at 1℃ $\cdot\, min^{-1}$, 1 hour soaking time, heating from 300℃ to 500℃ at 1℃ $\cdot\, min^{-1}$, 1 hour soaking time, heating from 500℃ to 1200℃ at 15℃ $\cdot\, min^{-1}$, 6 hours soaking time and natural cooling to room temperature).

Bulk density of green and sintered specimens was measured by mercury immersion (Archimedes' method), and their densification was calculated as the change in bulk density due to sintering divided by the change needed to attain a pore-free solid, according to German [40].

The pore size distribution as well as the total pore volume of the electrodes was measured through the mercury intrusion porosimetry technique (AutoPore® IV 9500, Micromeritics®, USA). An energy-dispersive X-ray (EDX) microanalysis instrument (Genesis 7000 SUTW; EDAX, Mahwah, NJ) coupled to a FEG-SEM (QUANTA® 200F, FEI® Co, USA, Hillsboro, OR) was used to determine the surface chemical composition and the microstructure of the samples. The electrical resistivity of sintered samples was measured with a resistance meter (RM 3545, Hioki® E.E. Corp. Japan), taking the average of ten measures for each specimen.

Electrochemical characterization

Five electrodes were electrochemically characterized in this work: the 3 ceramic electrodes synthetized in this work's context, a mirror polished Pt electrode, and a commercial 2500 ppm Nb-supported BDD electrode (neoCoat®, Japan). The electrochemical characterization of the electrodes was carried out in a conventional 3-electrode thermostatted electrochemical cell, using a 302N Autolab® potentiostat/galvanostat with FRA module, controlled with NOVA® software. The electrode to be characterised was used as the working electrode. In the case of the ceramic electrodes, the electrical contact with the prismatic shape was done using a platinum wire. The geometric surface of the working electrode was measured with high precision using a confocal laser scanning microscope (Olympus® LEXT OLS 3000, USA), before starting each electrochemical test. Though the exact geometric surface varied slightly from one working electrode to another, they were all in the 25 mm^2 range. A commercial Pt ring electrode (Crison® 5267) was used as the counter-electrode, and a commercial Ag/AgCl (3M KCl) electrode (Crison® 5240) was used as the reference electrode. All the experiments were done at 30ºC, using a 0.1 M Na_2SO_4 (Panreac® S.A., Spain) electrolyte.

First, cyclic voltametries (CVs) were performed in the anodic domain at 10 different scan rates, equally spaced from 100 $mV \cdot s^{-1}$ to 10 $mV \cdot s^{-1}$. Each voltammetry was carried out from the open circuit potential (OCP) to +4 V. For each scan rate, 30 cycles were measured in order to ensure the convergence of the voltammogram to the corresponding limit cycle. Then, the pseudo-steady-state polarization curve was measured from OCP to +4 V, at 1 $mV \cdot s^{-1}$. The aforementioned scan rate was selected in preliminary studies in which it was observed that this scan rate is slow enough in order to ensure that the steady-state is reached in every point.

Second, the electrochemical impedance spectrum (EIS) of the system was measured at 15 different overpotentials. EIS is an electrochemical technique that has been applied to a wide range of applications [41, 42]. Its main strength is that it allows to deconvolve the different physic-chemical processes undergoing at different timescales in the system [43]. In this work, EIS was used to obtain the uncompensated resistance of the system at different overpotentials, in order to correct the ohmic drop in the measured CVs. The main limitation of EIS is that its validity is restricted to situations in which causality, linearity and stability are achieved [44]. For this reason, validation is a fundamental part of the preliminary analysis of experimental EIS spectra. In this work, all the measured EIS spectra were double-validated: on the one hand, they were validated using the linearity assessment methods developed in previous works [45, 46]; and on the other hand, they were validated using the Kramers-Kronig based quantitative validation technique described in previous works [47, 48]. In this work, the EIS measurements were performed at 100 frequencies logarithmically spaced between 10 kHz and 10 mHz. The measurement parameters were selected using the methodology presented in a previous work [49]. Finally, since electrochemical systems are highly nonlinear systems [50, 51], the proper selection of the perturbation amplitude is crucial for fulfilling the linearity hypothesis. In this work, a perturbation amplitude of 20 mV was used for all the EIS measurements. This amplitude was selected using the selection methodology presented in previous works [52, 53].

The uncompensated resistance is given by the high frequency intersect of the EIS spectrum with the real axis [54]: in this work, the uncompensated resistance for each overpotential was determined from the high frequency intersect of the experimentally measured impedance spectrum at that overpotential with the real axis. Both, the CVs and the pseudo-steady-state polarization curve, were I-R corrected using the procedure described by Hrbac and co-workers [55], and the uncompensated resistances determined from EIS measurements.

Acknowledgements

The authors are very grateful to the Ministerio de Economia y Competitividad (Projects: CTQ2015-65202-C2-1-R and CTQ2015-65202-C2-2-R) and to the European Regional Development Fund (FEDER), for their economic support.

References

[1] R. P. Schwarzenbach, T. Egli, T. B. Hofstetter, U. Von Gunten, B. Wehrli, Annu. Rev. Environ. Resour. **2010**, 35, 109-136.
[2] M. A. Fard, B. Barkdoll, Electrochim. Acta **2018**, 265, 209-220.
[3] I. Oller, S. Malato, J. Sánchez-Pérez, Sci. Total Environ. **2011**, 409, 4141-4166.
[4] L. Yang, Z. Zhang, J. Liu, L. Huang, L. Jia, Y. Feng, ChemElectroChem **2018**, 5, 3451-3459.
[5] F. C. Moreira, R. A. R. Boaventura, E. Brillas, V. J. P. Vilar, Applied Cat. B: Environ. **2017**, 202, 217-261.
[6] O. Turkay, S. Barışçi, E. Ulusoy, M.G. Şeker, A. Dimoglo, Electrochim. Acta **2018**, 263, 400-408.
[7] A. Kouskouki, E. Chatzisymeon, D. Mantzavinos, Z. Frontistis, ChemElectroChem **2018**, DOI 10.1002/celc.201800971.
[8] D. Dionisio, A.J. Motheo, C. Sáez, P. Canizares, M. A. Rodrigo, ChemElectroChem **2018**, DOI 10.1002/celc.201801332
[9] A. J. dos Santos, C. A. Martínez-Huitle, I. Sirés, E. Brillas, ChemElectroChem **2018**, 5, 685-693.
[10] J. E. Silveira, A. L. Garcia-Costa, T. O. Cardoso, J. A. Zazo, J. A. Casas, Electrochim. Acta **2017**, 258, 927- 932.
[11] G. F. Pereira, B. F. Silva, R. V. Oliveira, D. A. C. Coledam, J. M. Aquino, R. C. Rocha-Filho, N. Bocchi, S. R. Biaggio, Electrochim. Acta **2017**, 247, 860- 870.
[12] R. M. Farinos, L. A. M. Ruotolo, Electrochim. Acta **2017**, 224, 32-39.
[13] H. Li, Y. Long, X. Zhu, Y. Tian, J. Ye, Electrochim. Acta **2017**, 246, 1121-1130.
[14] L. Li, Z. Huang, X. Fan, Z. Zhang, R. Dou, S. Wen, Y. Chen, Y. Chen, Y. Hu, Electrochim. Acta **2017**, 231, 354-362.
[15] B. P. Chaplin, Environ. Sci. Process. Impacts. **2014**, 16, 1182-1203.
[16] D. Yang, Y. Gu, X. Yu, Z. Lin, H. Xue, L. Feng, ChemElectroChem **2018**, 5, 659–664.
[17] S. Cotillas, J. Llanos, P. Cañizares, D. Clematis, G. Cerisola, M. A. Rodrigo, M. Panizza, Electrochim. Acta **2018**, 263, 1-7.
[18] J. M. Poyatos, M. M. Muñio, M. C. Almecija, J. C. Torres, E. Hontoria, F. Osorio, Water Air Soil Poll. **2010**, 205, 187-204.
[19] I. Sirés, E. Brillas, M. A. Oturan, M. A. Rodrigo, M. Panizza, Environ. Sci. Pollut. R. **2014**, 21, 8336-8367.
[20] D. Bejan, E. Guinea, N. J. Bunce, Electrochim. Acta **2012**, 69, 275-281.
[21] D. A. García-Osorio, R. Jaimes, J. Vazquez-Arenas, R. H. Lara, J. Alvarez-Ramirez, J. Electrochem. Soc. **2017**, 164, E3321-E3328.
[22] B. Fleszar, J. Poszyńska, Electrochim. Acta **1985**, 30, 31-42.
[23] J. Mora-Gomez, M. Garcia-Gabaldon, E. Ortega, M. J. Sánchez-Rivera, S. Mestre, V. Pérez-Herranz, Ceram. Int. **2018**, 44, 2216-2222.
[24] J. Grimm, D. Bessarabov, W. Maier, S. Storck, R. D. Sanderson, Desalination **1998**, 115, 295-302.
[25] B. Adams, M. Tian, A. Chen, Electrochim. Acta **2009**, 54, 1491-1498.

[26] E. R. Leite, J. A. Cerri, E. Longo, J. A. Varela, C. A. Paskocima, J. Eur. Ceram. Soc. **2001**, 21, 669-675.
[27] O. Scarlat, S. Mihaiu, G. Aldica, J. Groza, M. Zaharescu, J. Eur. Ceram. Soc. **2004**, 24, 1049-1052.
[28] O. Scarlat, S. Mihaiu, G. Aldica, M. Zaharescu, J. R. Groza, J. Am. Ceram. Soc. **2003**, 86, 893-897.
[29] S. Mihaiu, O. Scarlat, G. Aldica, M. Zaharescu, J. Eur. Ceram. Soc. **2001**, 21, 1801-1804.
[30] K. Rubenis, S. Populoh, P. Thiel, S. Yoon, U. Müller, J. Locs, J Alloy. Compd. **2017**, 692, 515-521.
[31] R. Yang, Z. L. Wang, J. Am. Ceram. Soc. **2006**, 128, 1466-1467.
[32] M. M. Lorente-Ayza, M. J. Orts, V. Pérez-Herranz, S. Mestre, J. Eur. Ceram. Soc. **2015**, 35, 2333-2341.
[33] M. M. Lorente-Ayza, S. Mestre, V. Sanz, E. Sánchez, Ceram. Int. **2016**, 42, 18944-18954.
[34] S. Ardizzone, G. Fregonara, S. Trasatti, Electrochim. Acta **1990**, 35, 263-267.
[35] T. Reier, M. Oezaslan, P. Strasser, ACS Catal. **2012**, 2, 1765-1772.
[36] R. Kötz, S. Stucki, B. Carcer, J. Appl. Electrochem. **1991**, 21, 14-20.
[37] C. Comninellis, Electrochim. Acta **1994**, 39, 1857-1862.
[38] J. N. Soderberg, A. C. Co, A. H. Sirk, V. I. Birss, J. Phys. Chem. B **2006**, 110, 10401-10410.
[39] B. Liu, C. Wang, Y. Chen, Electrochim. Acta **2018**, 264, 350-357.
[40] A. Bose, R. M. German in Sintering theory and practice, John Wiley & Sons, New York, **1996**.
[41] J. J. Giner-Sanz, E. M. Ortega, V. Pérez-Herranz, Fuel Cells **2017**, 17, 391-401.
[42] J. J. Giner-Sanz, E. M. Ortega, V. Pérez-Herranz, J. Power Sources **2018**, 379, 328-337.
[43] M. E. Orazem, B. Tribollet in Electrochemical Impedance Spectroscopy, John Wiley & Sons, New Jersey, **2008**.
[44] P. Agarwal, M. E. Orazem, L. H. Garcia-Rubio, J. Electrochem. Soc. **1995**, 142, 4159-4168.
[45] J. J. Giner-Sanz, E. M. Ortega, V. Pérez-Herranz, Electrochim. Acta **2015**, 186, 598-612.
[46] J. J. Giner-Sanz, E. M. Ortega, V. Pérez-Herranz, Electrochim. Acta **2016**, 211, 1076-1091.
[47] J. J. Giner-Sanz, E. M. Ortega, V. Pérez-Herranz, Int. J. Hydrogen Energ. **2015**, 40, 11279-11293.
[48] J. J. Giner-Sanz, E. M. Ortega, V. Pérez-Herranz, Electrochim. Acta **2016**, 209, 254-268.
[49] J. J. Giner-Sanz, E. M. Ortega, V. Pérez-Herranz, Electrochim. Acta **2015**, 174, 1290-1298.
[50] J. J. Giner-Sanz, E. M. Ortega, V. Pérez-Herranz, Fuel Cells **2015**, 15, 479-493.
[51] J. J. Giner-Sanz, E. M. Ortega, V. Pérez-Herranz, Int. J. Hydrogen Energ. **2014**, 39, 13206-13216.
[52] J. J. Giner-Sanz, E. M. Ortega, V. Pérez-Herranz, Fuel Cells **2016**, 16, 469-479.
[53] J. J. Giner-Sanz, E. M. Ortega, V. Pérez-Herranz, J. Electrochem. Soc. **2017**, 164, H918-H924.
[54] J. J. Giner-Sanz, E. M. Ortega, V. Pérez-Herranz, J. Power Sources **2018**, 381, 84-93.
[55] J. Hrbac, V. Halouzka, L. Trnkova, J. Vacek, Sensors **2014**, 14, 13943-13954.

Tables:

Table 1. Oxygen evolution reaction Tafel parameters

Electrode	$b\ (mV \cdot dec^{-1})$	$i_0\ (A \cdot cm_a^{-2})$
$(Sn, Sb, Cu)O + 0\%\ coke$	240	1.23×10^{-7}
$(Sn, Sb, Cu)O + 20\%\ coke$	240	3.70×10^{-7}
$(Sn, Sb, Cu)O + 40\%\ coke$	133	6.00×10^{-7}

Figures:

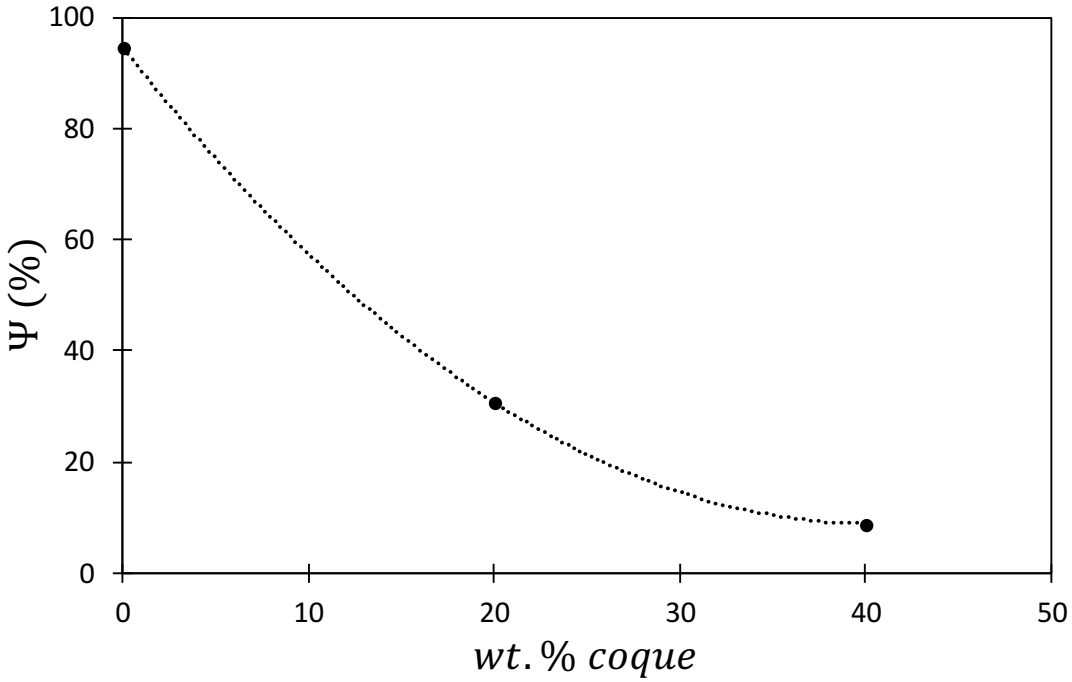

Figure 1. Densification of the sintered electrodes as a function of the amount of coke added before sintering

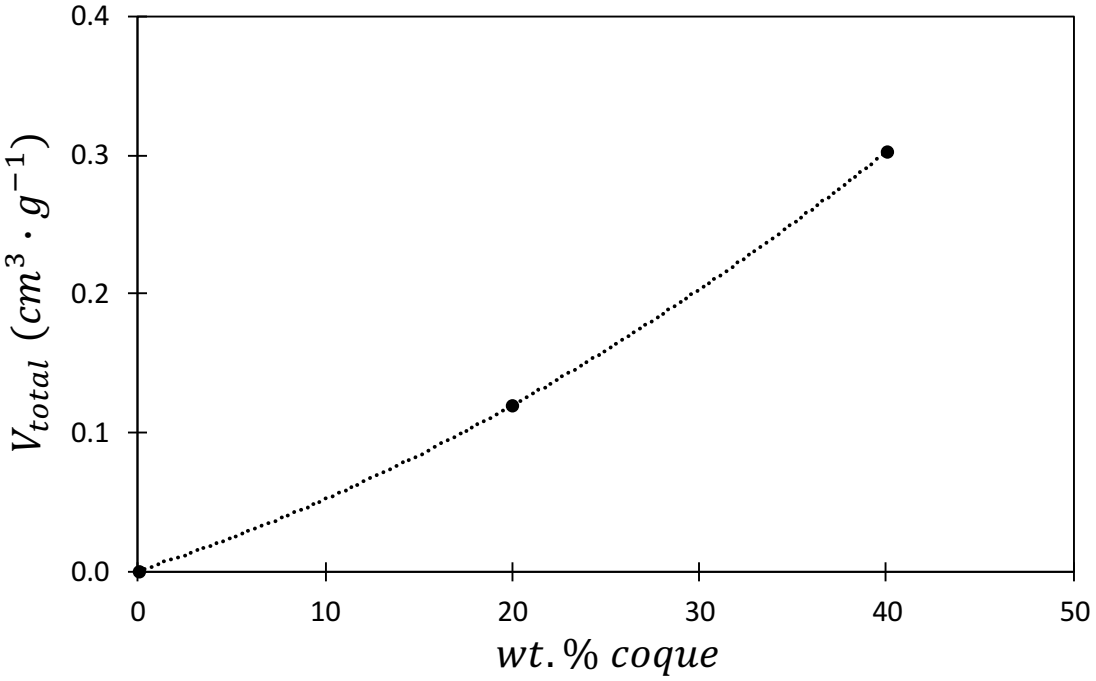

Figure 2. Total pore volume of the sintered electrodes as a function of the amount of coke added before sintering

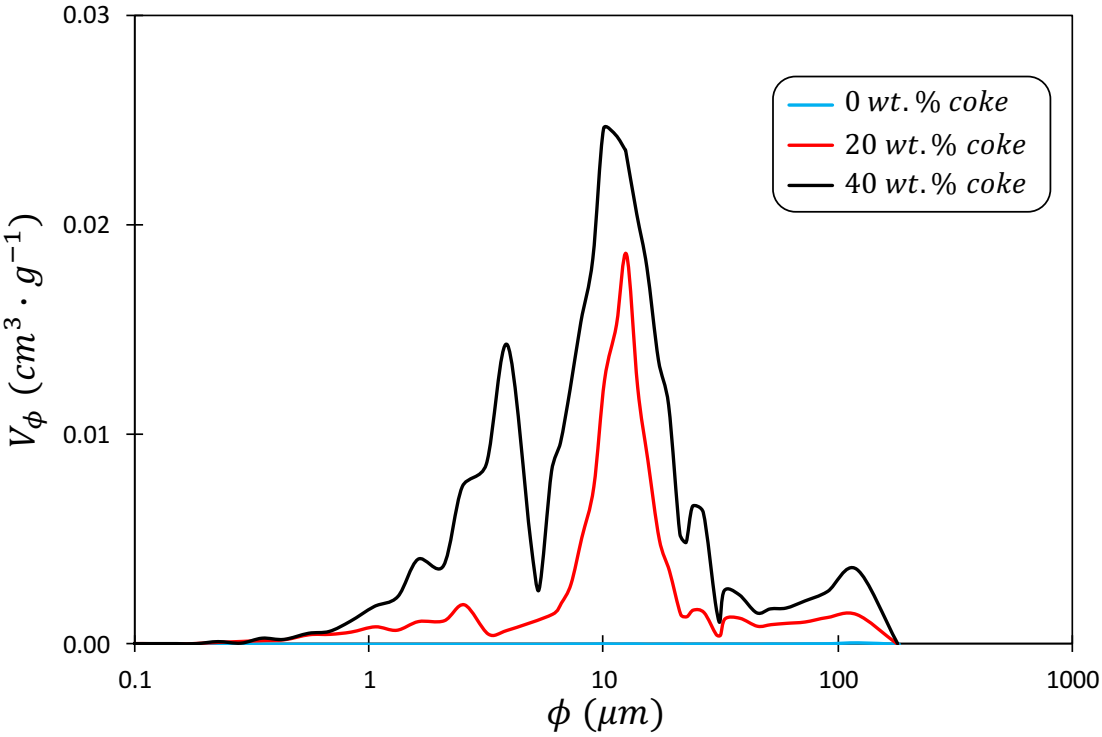

Figure 3. Pore distribution of the sintered electrodes for the different amounts of coke added before sintering

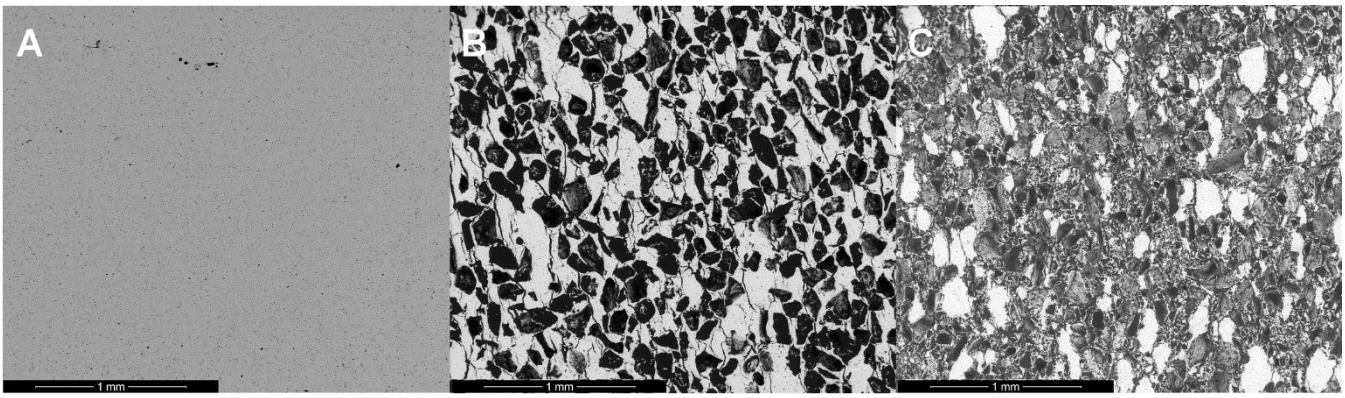

Figure 4. Microstructure of the sintered electrode as a function of the amount of coke added before sintering (A: 0 wt.% coke; B: 20 wt.% coke; C: 40 wt.% coke)

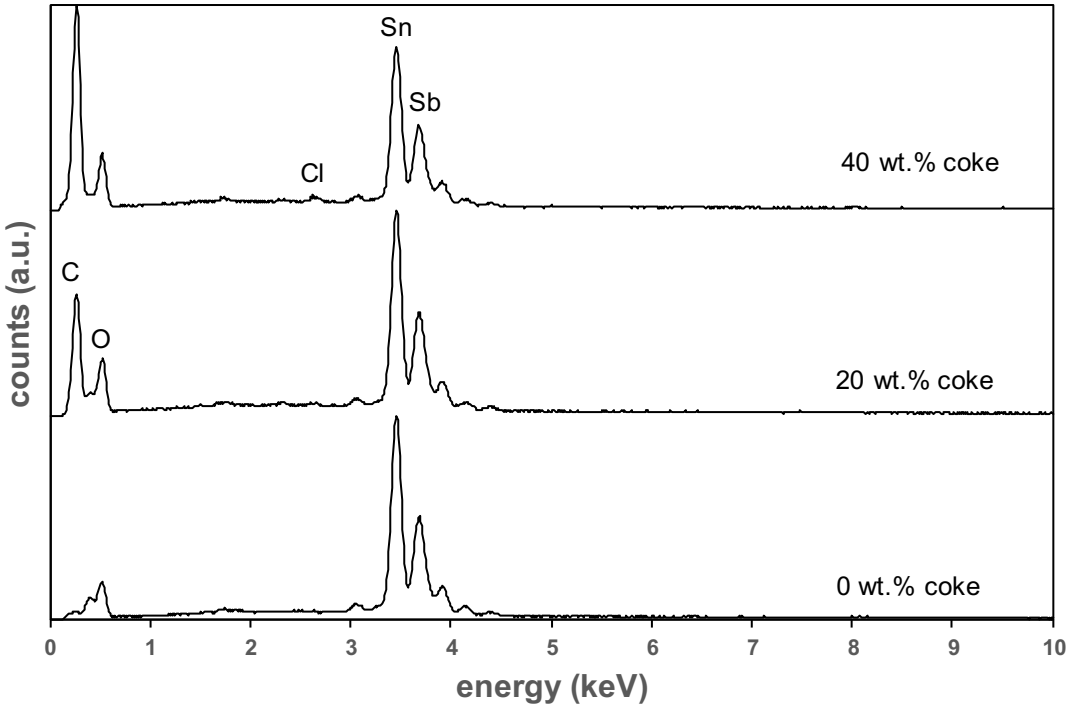

Figure 5. EDX spectra of polished sections of the different ceramic samples

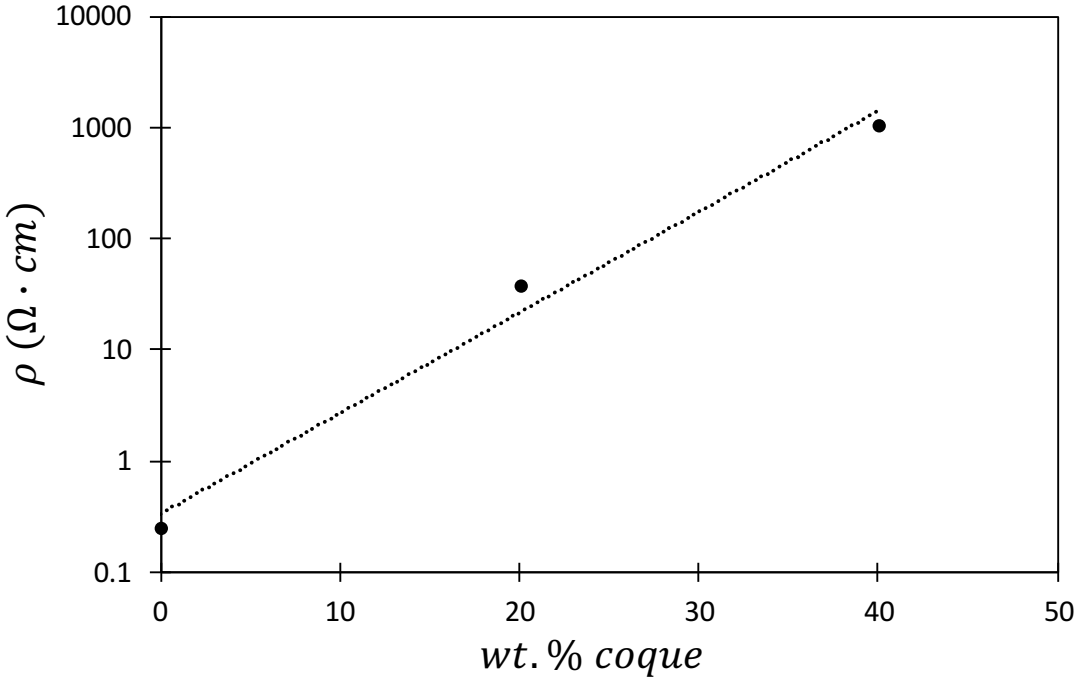

Figure 6. Electrical resistivity of the sintered electrodes as a function of the amount of coke added before sintering

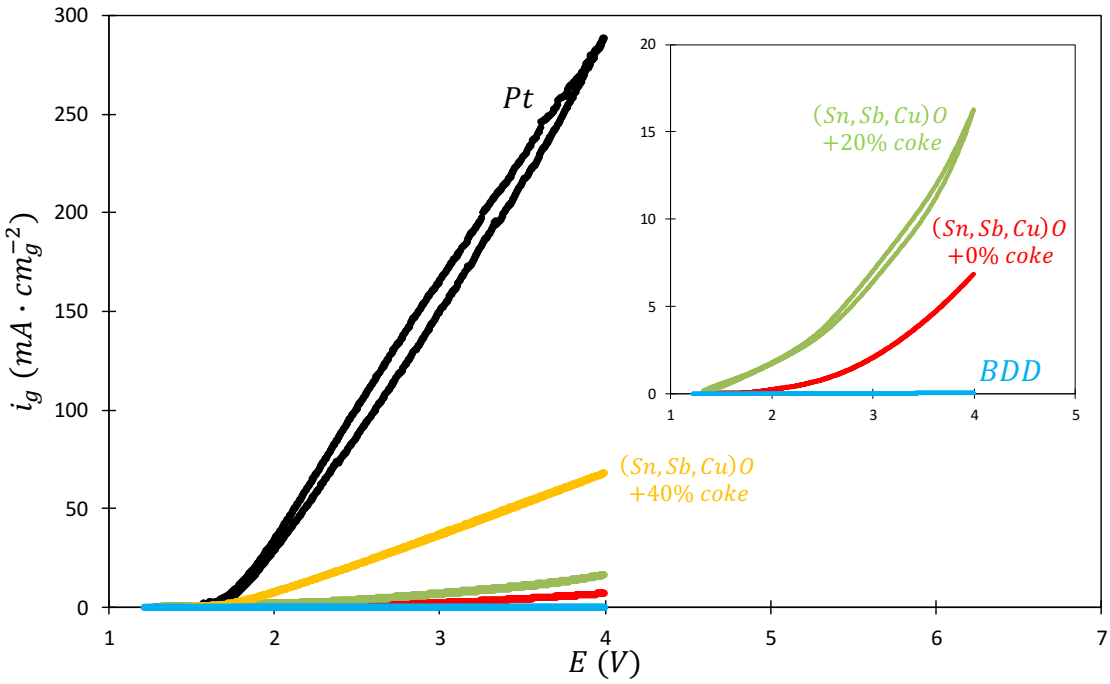

a.) Referred to geometric area

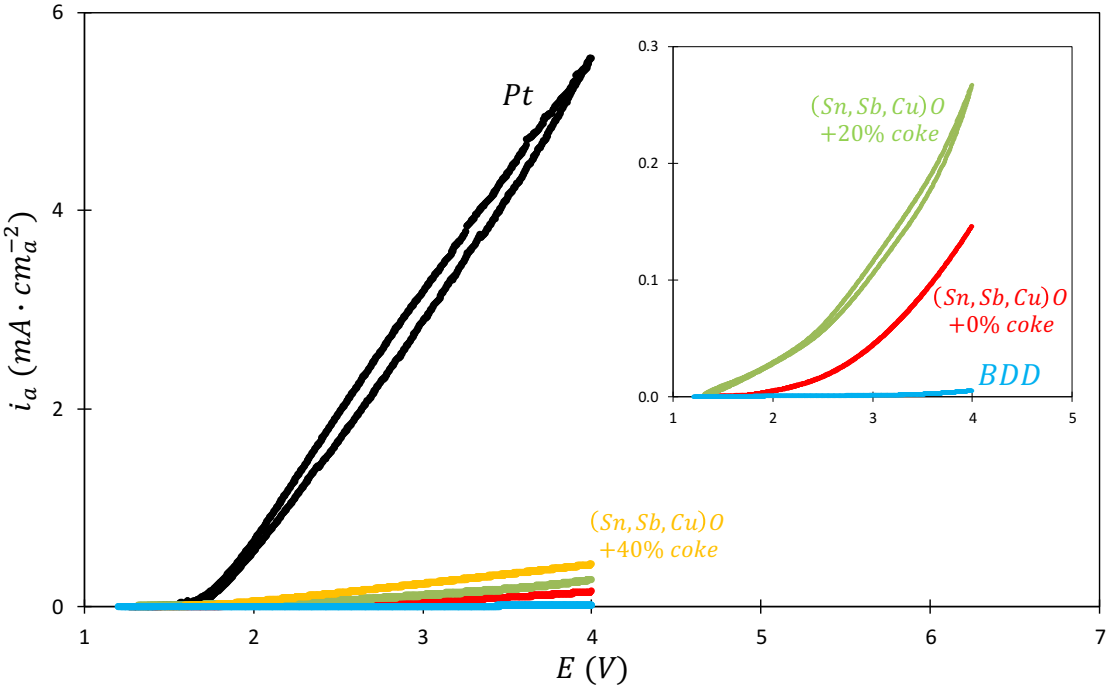

b.) Referred to active surface

Figure 7. Cyclic voltammetry curves obtained at a scan rate of $40\ mV \cdot s^{-1}$

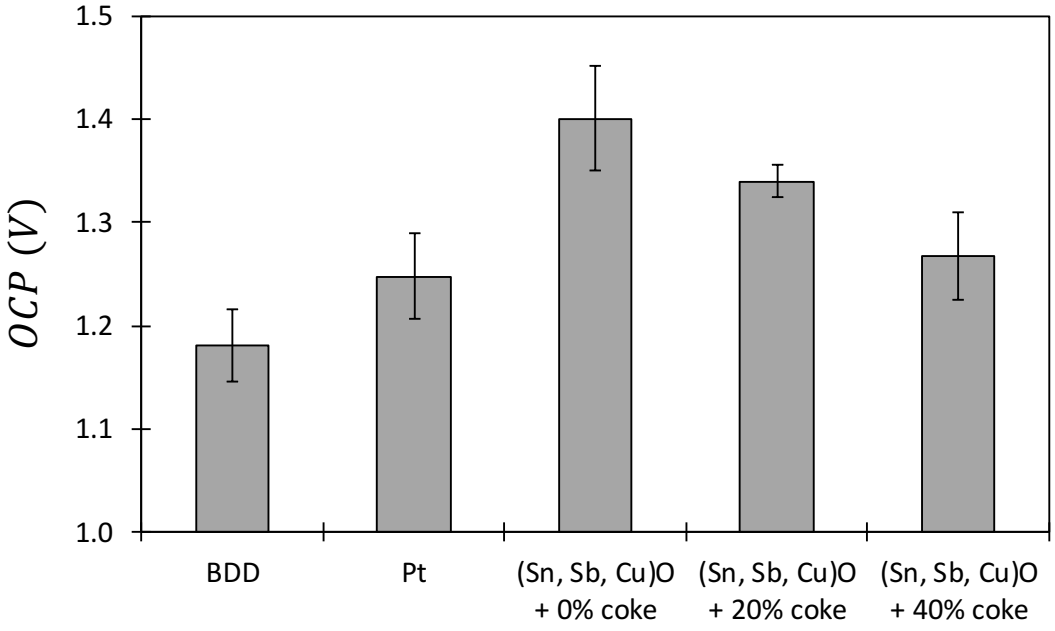

Figure 8. Open circuit voltage of the different anodes

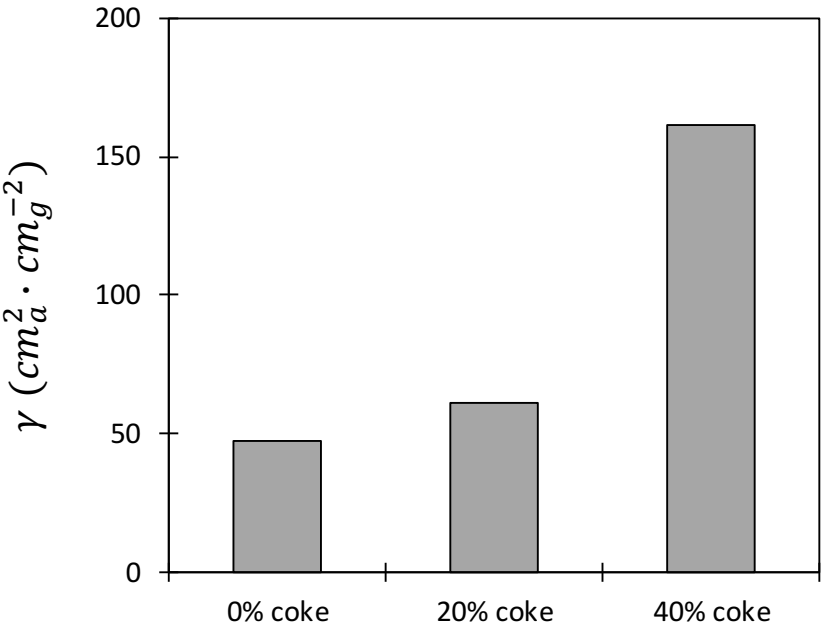

Figure 9. Electrochemical rugosity factor of the three ceramic anodes

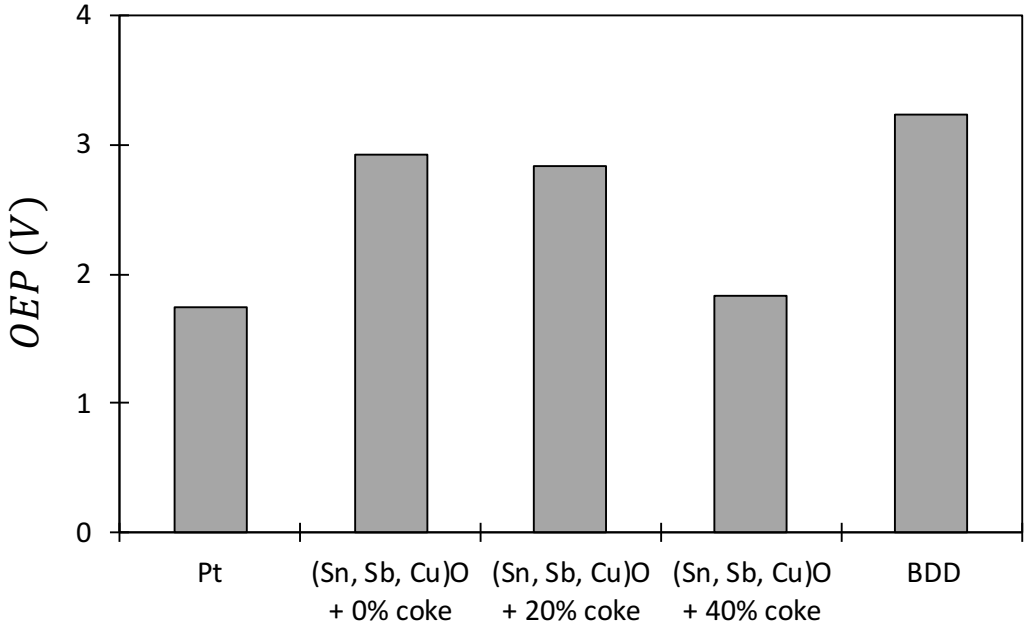

Figure 10. Oxygen evolution potential of the different anodes

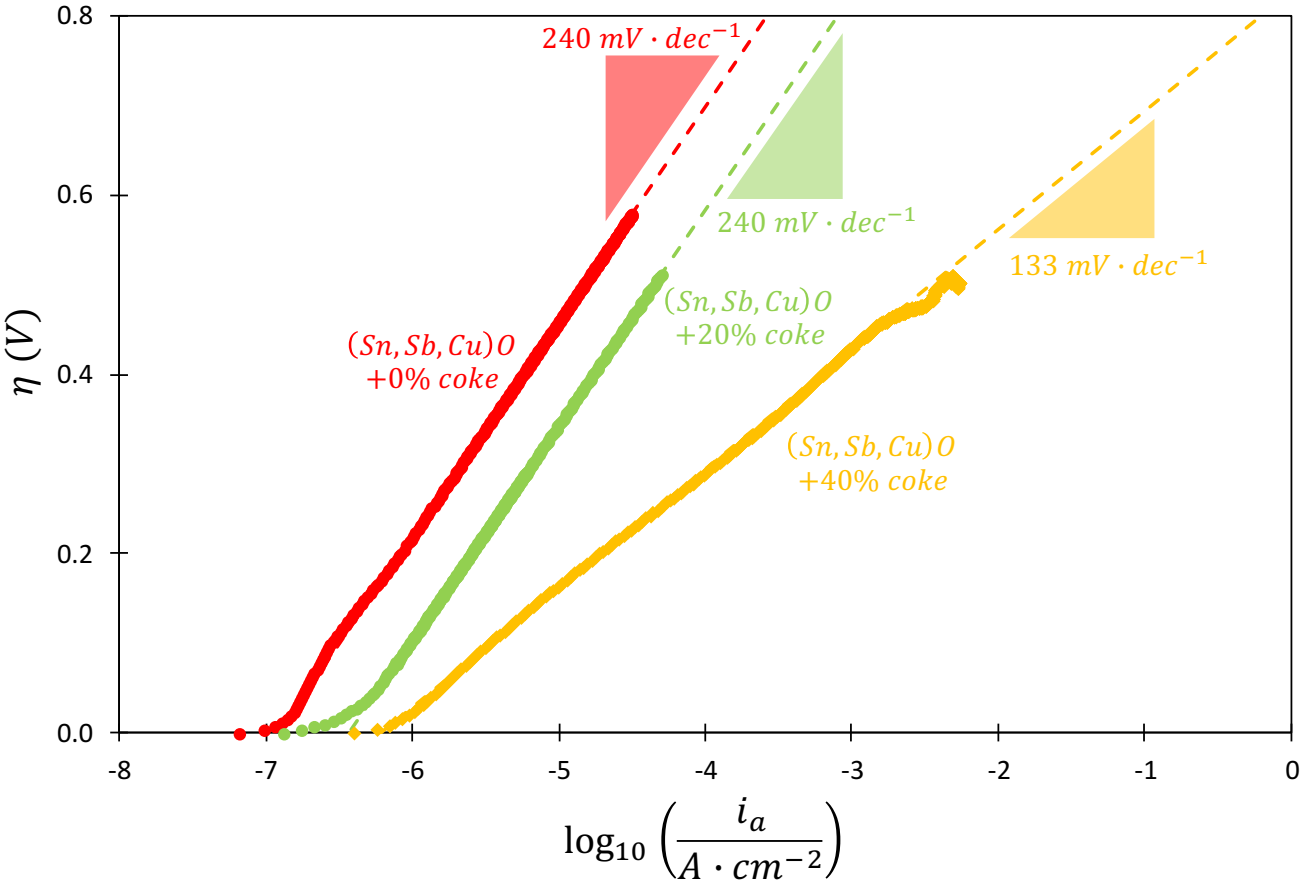

Figure 11. I-R corrected pseudo-steady-state polarization curves in the Tafel plot